Applied Surface Science 639 (2023) 158183

Contents lists available at ScienceDirect

Applied Surface Science

journal homepage: www.elsevier.com/locate/apsusc

Full Length Article

Simultaneously addressing self-stacking and oxidative degradation issues of $Ti_3C_2T_x$ MXene through biothermochemistry induced 3D crosslinking

Haitao Zhang [a,*], Hanyu He [a], Yongxiang Huang [b], Shi Pu [a], Yanting Xie [a], Junfeng Huang [a], Xinling Jiang [a], Yongbin Wang [a], Shenglong Wang [a], Hongzhi Peng [a], Yuanxiao Qu [a], Weiqing Yang [a,c]

[a] Key Laboratory of Advanced Technologies of Materials (Ministry of Education), School of Materials Science and Engineering, Southwest Jiaotong University, Chengdu 610031, China
[b] PLA Army Service Academy, No. 79 Yuzhou Road, Jiulongpo District, Chongqing 400041, China
[c] Research Institute of Frontier Science, Southwest Jiaotong University, Chengdu, 610031, China

ARTICLE INFO

Keywords:
$Ti_3C_2T_x$ MXenes
Biothermochemistry
3D crosslinking
Self-stacking
Oxidative degradation
Supercapacitors

ABSTRACT

As a recent rising star 2D material, MXenes have attracted great attention in many fields. However, the weak interaction induced self-stacking phenomenon and surface oxidation caused structure failure seriously hinder the practical application of MXenes. Herein we develop a biothermochemistry method to construct 3D crosslinked $Ti_3C_2T_x$ (3D-MX). This novel structured 3D-MX can be prepared in five different kinds of biological reagents, showing good university. After crosslinking, 3D-MX not only resists layer stacking but also exhibits extreme on-shelf stability up to 550 days. We reveal that the formation mechanism originates from the electrostatic/chemical interaction between surface functional groups and the crosslinking agents. Interestingly, the biothermochemical treated $Ti_3C_2T_x$ MXenes exhibit an extremely-rapid film-processed capability (only 3 min), addressing the long-standing issue of low-efficient and tedious solution-vacuum filtrated 2D films. To further verify its practical application, we assemble 3D-MX based supercapacitors that show a high specific capacitance of 265 Fg^{-1} at 1 A g^{-1}, and moreover, no supercapacitance attenuation within 720 h. This proposed biothermochemistry method to simply and rapidly build 3D $Ti_3C_2T_x$ crosslinked network provides a new perspective to promote the practical application of MXenes through simultaneously addressing their self-stacking and oxidative degradation issues.

1. Introduction

Since the beginning of 21st century, two-dimensional (2D) nanomaterials, such as graphene, MoS_2, and black phosphorus [1–3], have received great interests in many fields. Among them, a new family named "MXenes" has attracted much attention due to its high conductivity [4], plentiful terminal groups [5], good hydrophilicity [6] and so on. The general formula of MXenes is $M_{n+1}X_nT_x$, where M means an early transition metal such as Ti, V, Cr, Nb, Mo, X refers to nitrogen and/or carbon, T_x stands for the terminal groups such as = O, -F, –OH, and n commonly equals to 1–3 [7]. To this day, more than 20 members of MXenes have been synthesized, among which $Ti_3C_2T_x$ is the most studied by far. Benefited by its unique composition, $Ti_3C_2T_x$ shows a great application prospect including energy storage [8], electromagnetic interference shielding [9], water purification [10], and many others, owing to excellent electrical conductivity (~20,000 S cm^{-1}) [11], hydrophilic surfaces, high flexibility, and other outstanding features [12].

Unfortunately, there are still some challenges impeding the practical application of $Ti_3C_2T_x$. On the one hand, many researchers have found that $Ti_3C_2T_x$ will oxidize very quickly along with serious structural damage when contacting with air or/and water in a few days observed by direct color variation from black/dark green to white [13]. Recent research suggested that $Ti_3C_2T_x$ would convert into titanium dioxide (TiO_2) and carbon (C) when preserved in water for several days, which was proved by transmission electron microscopy (TEM) characterization [14]. The degradation of $Ti_3C_2T_x$ involves many factors like temperature, water, and heating rate [15,16]. And it would start at the edges then expand inward gradually. Also, the degradation is related to the size of the nanosheets [17], with the large flakes being most stable because the stack formed by multi-layer structure reduces the overall

* Corresponding author.
E-mail address: haitaozhang@swjtu.edu.cn (H. Zhang).

https://doi.org/10.1016/j.apsusc.2023.158183
Received 21 May 2023; Received in revised form 19 July 2023; Accepted 5 August 2023
Available online 6 August 2023

specific surface area and thus reduces the contact with water and oxygen. Furthermore, the stronger effect of water than oxygen on oxidation of $Ti_3C_2T_x$ lies that the protonated hydroxyl terminal groups of $Ti_3C_2T_x$ flakes can make Ti atoms more electrophilic and bare Ti atoms are vulnerable to attack by oxidation factors to generate TiO_2 [18]. Since the most excellent properties of $Ti_3C_2T_x$ will be greatly declined after oxidative degradation, it is urgent to develop the preservation and antioxidant strategies.

At present, there are three main methods to deal with the oxidative degradation of $Ti_3C_2T_x$. The first method is physical protection, including storing $Ti_3C_2T_x$ in a low-temperature environment, using organic reagents as solvents [19] and applying a protective layer to its surface [20]. However, cryopreservation and the use of organic solvents only slow down the oxidation of $Ti_3C_2T_x$. For example, Shang reported a physical packaging method by coating the surface of $Ti_3C_2T_x$ with a layer of metal oxide to slow down the oxidation rate. However, due to the presence of low conductivity functional groups or metal oxides, the conductivity of $Ti_3C_2T_x$ decreased sharply [21]. The second method is chemical method including improvement of synthesis process and heat treatment. Mathis et al. added excessive aluminum during the synthesis of Ti_3AlC_2 MAX precursor to improve the crystallinity of the grains, allowing $Ti_3C_2T_x$ to be stored in water for over 10 months [22]. Unstable functional groups on the surface of $Ti_3C_2T_x$ are removed by annealing in atmospheres such as hydrogen and ammonia to improve oxidation stability [23–25]. But the disadvantage of this method lies that it cannot process $Ti_3C_2T_x$ colloidal solutions, consuming a lot of energy and increases the stacking of $Ti_3C_2T_x$ layers. The third method is biological reagent protection. Zhao and co-authors used L-ascorbate to protect $Ti_3C_2T_x$ nanosheets [26]. Due to the combination of L-ascorbic acid and the edge of nanosheets, the contact area with water and oxygen was reduced, making it not significantly degraded when stored in aqueous solution for 21 days. Wu et al. used sodium ascorbate to protect $Ti_3C_2T_x$, which could be stored at room temperature and in air for over 80 days [27]. Varun Natu et al. used polyanions such as polyphosphates and polyciliate to protect $Ti_3C_2T_x$ nanosheets, which enabled them to be stored in water for several weeks without significant oxidation [28]. Therefore, resorting to proper strategy, the oxidative problem of MXenes would be unlocked.

On the other hand, MXenes themselves are one kind of 2D materials with no support between layers. Surface functional groups would cause self-stacking between layers based on electrostatic interactions, which is particularly serious during film formation, and therefore leading to a decrease in surface active sites and affect many properties [29]. To solve this self-stacking problem, intercalation agents are mostly introduced to expand the layer spacing [30]. For example, Yang et al. interlaced porous carbon with the $Ti_3C_2T_x$ surface to increase the contact area to improve electron transfer efficiency, while also serving as a spacer to alleviate stacking [31]. Xue et al. reduced stacking by adding polyaniline nanoparticles between $Ti_3C_2T_x$ nanosheets as an embedding agent [32].

Although many methods have been adopted, there is still a lack of simultaneous solutions to the oxidation and self-stacking problems of $Ti_3C_2T_x$. Using intercalation agents to solve the self-stacking problem of $Ti_3C_2T_x$ is often difficult to maintain long-term stability; The introduction of antioxidants and other methods often fails to effectively expand interlayer spacing. Therefore, it holds the primary importance to find an efficient and simple method to solve the two above-mentioned problems.

Here, we report a biothermochemistry method to form a 3D crosslinked $Ti_3C_2T_x$ network to simultaneously inhibit oxidative degradation and self-stacking. Five biological reagents including glutathione, tannic acid, sodium citrate, sodium alginate, and phytic acid have been proved to successfully build 3D network structures. On the one hand, the layer spacing of $Ti_3C_2T_x$ was expanded as indicated by a 2-theta shifts down from 6.4° to 5.0° of (0 0 2) diffraction peak; On the other hand, the crosslinked $Ti_3C_2T_x$ colloidal solution exhibited excellent oxidation stability, and the color remains black up to 550 days while the untreated $Ti_3C_2T_x$ turned completely white only within 30 days. Meanwhile, the modified $Ti_3C_2T_x$ based supercapacitors show almost no attenuation and show a capacitance of 265 F g^{-1} at a current density of 1 A g^{-1}. In contrast, the crosslinked-free $Ti_3C_2T_x$ decreases by 19% in capacitance after 30 days.

2. Experimental section

2.1. Materials

Ti_3AlC_2 precursor powder (99.8 wt%, 11 Technology Co. Ltd, China), hydrochloric acid (HCl, 12 mol L^{-1}, Aladdin), lithium fluoride (LiF, 99.9 wt%, Aladdin), glutathione (Reduced) (G-SH, 98 wt%, Aladdin), tannic acid (UPS, Aladdin), sodium alginate (UPS, Aladdin), sodium citrate dihydrate (99 wt%, Aladdin), phytic acid solution (50% in H_2O, Aladdin).

2.2. Synthesis of $Ti_3C_2T_x$ MXene

$Ti_3C_2T_x$ MXene was prepared by etching Ti_3AlC_2 precursor with HCl and LiF [33]. Specifically, adding 2 g LiF to 40 mL of 9 mol L^{-1} HCl solution, and stirring the mixtures for 30 min. Then, 2 g Ti_3AlC_2 was added to the above-obtained solution, followed by transferring the mixed solution to a water bath pot to stir and etch at 40 ℃ for 24 h. The etching product was washed with an appropriate amount of ultrapure water. Then the supernatant was centrifuged to remove LiF, and the process was repeated about 6 times to make the pH of the solution reach ~ 7. After that, the etched $Ti_3C_2T_x$ solution was filtered to obtain solid products and then transferred to a vacuum oven at 40 ℃ for 24 h to further remove the moisture. Finally, $Ti_3C_2T_x$ MXene powders were grinded and collected for later use. The micromorphological characteristics of Ti_3AlC_2 precursor powder and $Ti_3C_2T_x$ MXene were shown in Figure S1.

2.3. Preparation of 3D-MX

0.1 g $Ti_3C_2T_x$ MXene was dissolved in 20 mL deionized water, and then conducted ultrasonic treatment for 1 h and centrifuged (3500 rpm) for 1 h to obtain MXene suspension. After that, 0.05 M glutathione, 0.05 M sodium citrate dihydrate, 0.05 M phytic acid, 0.02 M sodium alginate and 0.02 M tannins acid (named separately as 3D-MX-G, 3D-MX-SCD, 3D-MX-PA, 3D-MX-SA, 3D-MX-TA) were separately added to the suspension and stirred vigorously in ampullas. Then, transferring the $Ti_3C_2T_x$ solution containing different reagents to the oven for further heating at 75 ℃ for 12 h. Later, a proper amount of ultrapure water was added for washing and vacuum assisted filtration to obtain self-standing MXene films and further vacuum dried at 40 ℃ for 12 h. In contrast, in addition to different reagents and heating treatment in the later stage, pure $Ti_3C_2T_x$ MXene films (named as P-MX) with the same concentration and conditions were prepared by direct ultrasound, centrifugation, filtration and dehydration. The films after ultrasonic, centrifugation, heating for 12 h, filtration and dehydration were marked as t-MX. 3D-MX-G and t-MX films stored at room temperature and air environment for Y (Y = 1, 4, 7, 14 and 30) days are named 3D-MX-G-YD and t-MX-YD. And the detailed information of all the samples is summarized in Table 1.

2.4. Characterizations

X-ray photoemission spectroscopy (XPS, Thermo ESCALAB 250Xi) and elemental analysis (EA, vario EL CUBE, elemental) were used to prove the successful crosslinking between glutathione and $Ti_3C_2T_x$. Avantage software was used for analysis and processing as the previous XPS data. X-ray diffraction (XRD, DX-1000 diffractometer), scanning electron microscopy (SEM, JSM-7800F), energy dispersion spectroscopy

Table 1
The detailed information of the prepared samples.

Sample names	Biological reagent	Concentration (M)	Temperature (°C)	Reaction time (h)	Storage time (d)[5]
P-MX	/	/	/	/	/
P-MX-30D	/	/	/	/	30
t-MX	/	/	75	12	/
t-MX-1D	/	/	75	12	1
t-MX-4D	/	/	75	12	4
t-MX-7D	/	/	75	12	7
t-MX-14D	/	/	75	12	14
t-MX-21D	/	/	75	12	21
t-MX-30D	/	/	75	12	30
3D-MX-SA	SA[1]	0.02	75	12	/
3D-MX-SCD	SCD[2]	0.05	75	12	/
3D-MX-PA	PA[3]	0.05	75	12	/
3D-MX-TA	TA[4]	0.02	75	12	/
3D-MX-G	Glutathione	0.05	75	12	/
3D-MX-G-1D	Glutathione	0.05	75	12	1
3D-MX-G-4D	Glutathione	0.05	75	12	4
3D-MX-G-7D	Glutathione	0.05	75	12	7
3D-MX-G-14D	Glutathione	0.05	75	12	14
3D-MX-G-21D	Glutathione	0.05	75	12	21
3D-MX-G-30D	Glutathione	0.05	75	12	30
3D-MX-G-550D	Glutathione	0.05	75	12	550

Note: [1]SA is sodium alginate, [2]SCD is sodium citrate dihydrate, [3]PA is phytic acid, [4]TA is tannins acid, and [5]d represents day.

(EDS, JSM-7800F) and TEM (JEM-2100F) were used to obtain the morphologies and microstructures. The contact angle was collected with sessile drop method using DSA25 (KRUSS, Germany). The electroconductivity of different MXene films were obtained using a digital four probe tester (ST-2258C, JGR). Zeta potentials (Malvern, ZEN3690) of different MXene colloidal solutions were obtained by using a highly sensitive zeta potential and particle size analyzer.

2.5. Electrochemical measurements

All MXene film electrodes were tested using a three-electrode system to evaluate their electrochemical performance. In the three-electrode

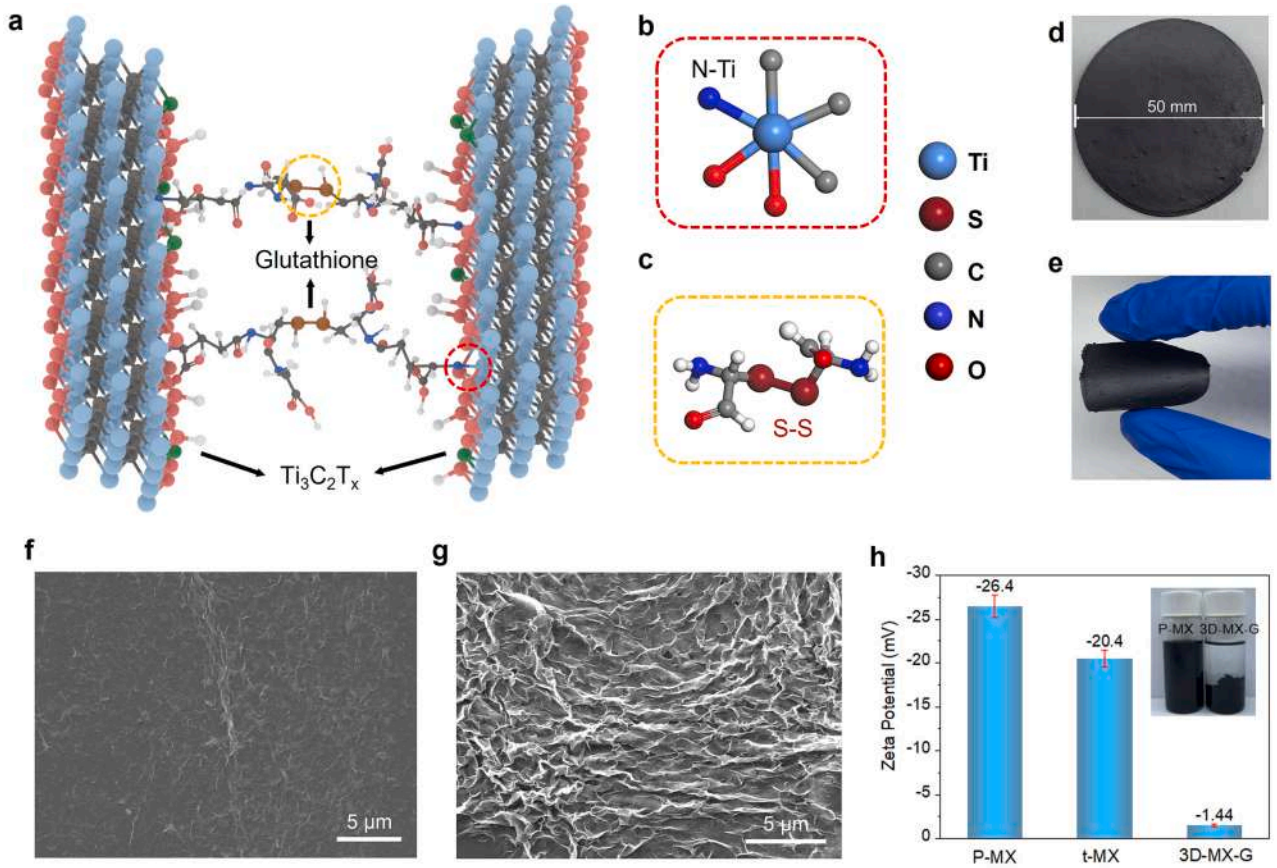

Fig. 1. Formation of 3D crosslinked structures. (a) Schematic diagram of 3D crosslinked structure formation of 3D-MX-G. (b) Formation of the Ti-N bond between $Ti_3C_2T_x$ and glutathione. (c) Formation of the S-S bond between glutathione. (d) The optical image of 3D-MX-G film. (e) The 3D-MX-G film image after bending. (f, g) SEM images of P-MX and 3D-MX-G. (h) Zeta potential of P-MX, 3D-MX-G, and t-MX.

system, the working electrode was the MXene film, the counter electrode is activated carbon, and the reference electrode was Hg/Hg_2SO_4. The 1 M H_2SO_4 solution was used as the electrolyte. Cyclic voltammetry (CV) (voltage range is set as −0.7–0.1 V), galvanostatic charge/discharge (GCD) and electrochemical impedance spectroscopy (EIS) with a frequency range from 0.1 Hz to 100 kHz tests were conducted on the electrochemical workstation (CHI660E, Chenhua, Shanghai).

2.6. Calculation

The gravimetric specific capacitances (C_m, F g^{-1}) from the GCD curves were calculated by the following equation [34]:

$C_m = It/\Delta Vm$ (1).where I is discharge current (A), t is discharge time (s), ΔV is the potential change in discharge process (V), and m is the mass of the working electrode (g).

3. Results and discussion

The schematic diagram of 3D crosslinked $Ti_3C_2T_x$ structure construction involving glutathione (3D-MX-G) was shown in Fig. 1**a**. During the biothermochemistry treatment process, the hydroxyl functional groups on the surface of $Ti_3C_2T_x$ were easily removed due to their instability, resulting in the exposure of Ti atoms. Then, glutathione combines with exposed Ti atoms via amino groups (–NH_2) to form Ti-N chemical bonds (Fig. 1b). At the same time, the sulfhydryl groups (-SH) between glutathione reacted with other groups such as oxidation factors to form disulfide bonds (-S-S-), thus connecting with each other (Fig. 1c). With the help of Ti-N bonds and S-S bonds, many $Ti_3C_2T_x$ nanosheets were interconnected to form a 3D crosslinked structure. The film forming property of $Ti_3C_2T_x$ was not affected by the crosslinked structure, and after small angle bending, it restored its original appearance, displaying good flexibility (Fig. 1d, 1e, S2).

The SEM was used to observe the surface morphology changes of 3D-MX-G before and after biothermochemical treatment. Fig. 1f shows the surface morphology of untreated $Ti_3C_2T_x$ (P-MX) that the nanosheets are scattered and presented an overall disordered state, with many nanosheets stacked in the middle to form ridges. After biothermochemistry treatment, many nanosheets in 3D-MX-G crosslinked to each other to form an apparent 3D network, resulting in a reduction in contact area with water or oxygen to inhibit oxidation (Fig. 1g).

Furthermore, the surface of 3D-MX-G films still maintained this stable and extensive 3D crosslinked structure, while cracks and particles appeared on the surface of P-MX film, indicating that the structure had been damaged (Figure S3). EDS shows that N and S elements are relatively uniformly distributed on the surface of 3D-MX-G, which to some extent proves the successful crosslinking effect from glutathione (Figure S4). Fig. 1h exhibits zeta potential diagrams of P-MX, 3D-MX-G and t-MX. Due to the presence of some terminal groups (–OH, -F, and = O) on the surface of $Ti_3C_2T_x$ nanosheets, the nanosheets exhibit negative charge. Therefore, the change of zeta potential reflects the change of surface charge to a certain extent. Compared to P-MX, zeta potential value of t-MX was reduced by 22.7%, which was attributed to the decline of surface functional groups caused by oxidation. Meanwhile, the zeta potential of 3D-MX-G dropped sharply by 94.5% and the nanosheet exhibited an apparent settling phenomenon, which was the result of the crosslinking effect between $Ti_3C_2T_x$ and glutathione.

To further prove the crosslinking effect between glutathione and $Ti_3C_2T_x$, we characterized the chemical composition and interface interaction of P-MX and 3D-MX-G by XPS characterization (Fig. 2). Fig. 2a shows the Ti 2p, O 1 s, and C 1 s core-level spectra of P-MX and

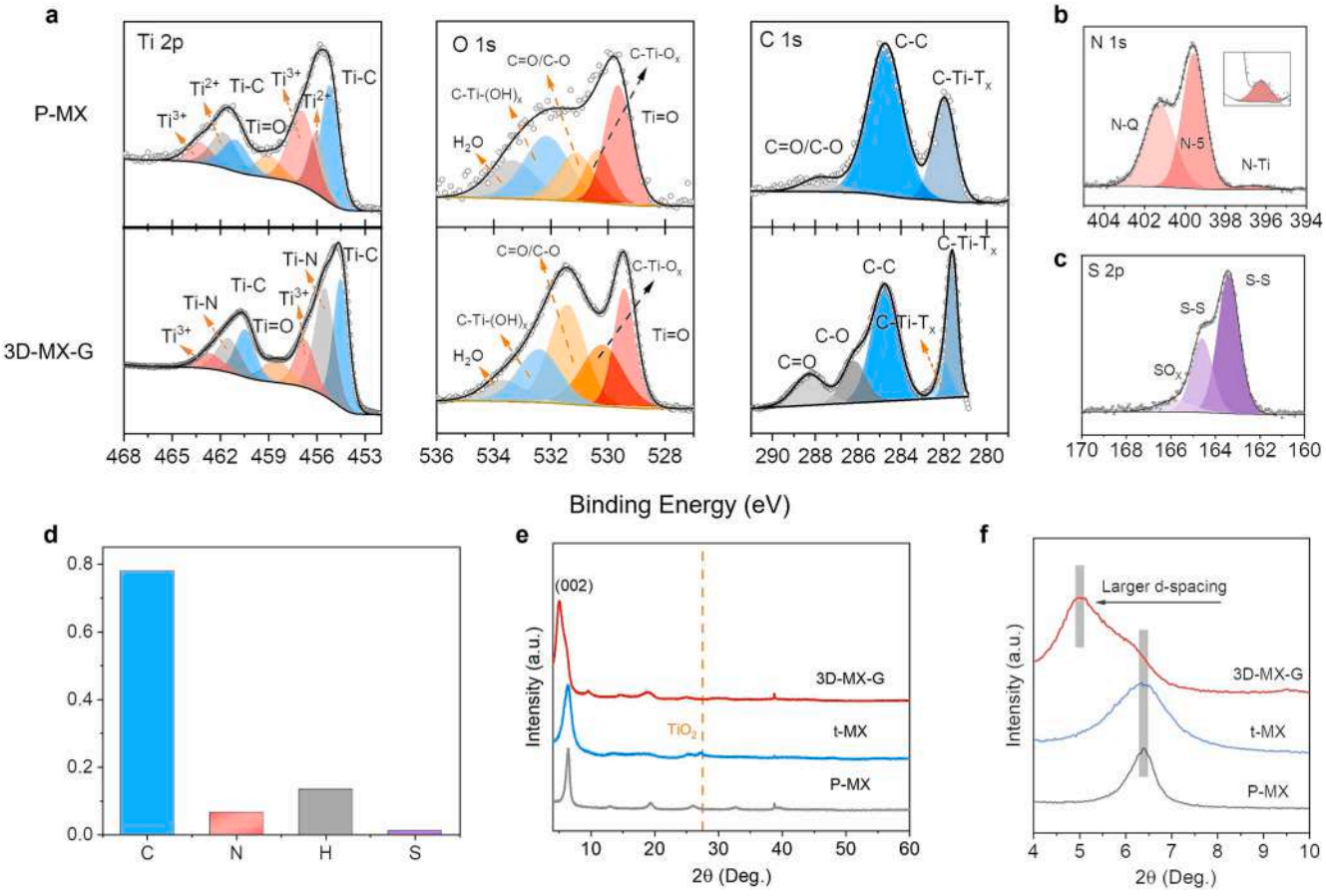

Fig. 2. The crosslinking interaction of 3D-MX-G. (a) XPS spectrum of P-MX and 3D-MX. (b) XPS spectrum of N for 3D-MX-G. (c) XPS spectrum of S for 3D-MX-G. (d) Percentage of element content of 3D-MX-G. (e) XRD patterns for P-MX, t-MX and 3D-MX-G. (f) The enlarged part of Figure (e).

3D-MX-G. In Ti 2p spectra, compared with P-MX, the percentage change of Ti-C (460.4/454.5 eV) content was not very apparent while the content of Ti^{2+} (461.4/455.4 eV) increased from 24% to 38% (Figure S5a) due to the reduction of glutathione, implying the reduction of high valence state of Ti atoms on the surface of $Ti_3C_2T_x$ [35,36]. The proportion of Ti^{3+} content in 3D-MX-G was decreased from 32% to 17%, which was beneficial to reducing the possibility of oxidation. Moreover, the change in the content of Ti = O bonds was not significant after the formation of the 3D network structure, indicating a significant inhibitory effect of glutathione on its oxidation. O 1 s spectra of 3D-MX-G was deconvoluted into five components located at 529.4, 530.2, 531.4, 532.4 and 533.6 eV, which assign to the Ti = O, C-Ti-O_x, C = O/C-O, C-Ti-$(OH)_x$ and H_2O, respectively [37]. The content of C-Ti-$(OH)_x$ has decreased to a certain extent (Table S1, S2) because the reduction effect of glutathione that reduces the hydroxyl groups on the surface of $Ti_3C_2T_x$. In C 1 s spectrum, the peak area of C-Ti-T_x (281.5 eV) of both 3D-MX-G and P-MX was similar [38]. The core energy level spectra of fitted N 1 s (Fig. 2b) shows three components centered at 396.7, 399.6, and 401.3 eV that are assigned to N-Ti, pyrrole-N (N-5), and graphite-N (N-Q) bonds, respectively (Figure S5b) [39–41]. In N 1 s spectrum, the interaction between glutathione and $Ti_3C_2T_x$ was originated from Ti-N bonds. The spectrum of the S 2p was divided into three peaks around 163.4, 164.6 and 165.8 eV that were attributed to the $2p_{3/2}$, $2p_{1/2}$ of the S-S and S-O bonds (Fig. 2c) [42,43]. Based on these results, it is reasonable to infer that the 3D crosslinked structure of 3D-MX-G was formed through Ti-N and S-S chemical bonds.

EA was utilized to prove the crosslink effect between glutathione and $Ti_3C_2T_x$ (Fig. 2d). The test showed that the film of 3D-MX-G contained about 6.62% N and 1.08% S elements (Table S3), implying the potential formation of chemical bonds between $Ti_3C_2T_x$ and glutathione since the 3D-MX-G was further washed by deionized water. Fig. 2e shows the XRD patterns of P-MX, t-MX and 3D-MX-G. Compared to P-MX, the (002) diffraction peak of 3D-MX-G shifts from 6.4° to 5.0°, demonstrating that the increase in layer spacing due to the presence of pyrrole-N (N-5) and graphite-N between $Ti_3C_2T_x$ and glutathione, while there was almost no shift in t-MX. The peaks at about 27.5° was attributed to the rutile TiO_2 (JCPDS #12–1276), and the rutile TiO_2 had a strong structural destruction effect on $Ti_3C_2T_x$ [28,44]. Compared to P-MX, the higher and wider peak of rutile TiO_2 in t-MX indicated more structural damage, while the absence of this peak in 3D-MX-G implied that glutathione played a protective effect on the structure of $Ti_3C_2T_x$. The excellent oxidation stability of 3D-MX-G could be described as following. In the process of biothermochemistry, on the one hand, the amino functional group on the surface of free glutathione formed stable Ti-N chemical bonds with the bare Ti atoms on the surface of $Ti_3C_2T_x$, preventing the attack of oxidation factors on the Ti atoms. Meanwhile, glutathione, as a natural reducing agent, also removed unstable hydroxyl groups on the surface of $Ti_3C_2T_x$ and formed Ti-N bonds with Ti atoms, effectively reducing the oxidation initiation sites; On the other hand, the sulfhydryl groups on glutathione reacted with each other to form S-S bonds, thereby crosslinking $Ti_3C_2T_x$ to form a 3D network structure and improving overall stability.

Moreover, we prove that this biothermochemistry method holds the universality to prepare 3D-MX. As shown in Fig. 3, sodium alginate, sodium citrate dihydrate, phytic acid and tannins acid (Fig. 3a_1-d_1) also construct other four 3D-MX to inhibit the self-stack of $Ti_3C_2T_x$. Interestingly, $Ti_3C_2T_x$ nanosheets in 3D-MX-SA, 3D-MX-SCD and 3D-MX-PA were deposited to the bottom (Fig. 3a_2, 3b_2 and 3c_2), while the colloidal solution of 3D-MX-TA presented a stable and uniform black color after biothermochemical treatment (Fig. 3d_2). All these treated colloidal solutions could be formed MXene films (Fig. 3a_3-d_3). The surfaces of four typed $Ti_3C_2T_x$ exhibited different forms of 3D crosslinked networks (Fig. 3a_4-d_4), with varying degrees of expansion in interlayer spacing (2-theta shifted down from 6.4° to 5.5° of (002) diffraction peak) (Figure S6), indicating that the universal construction of 3D crosslinked networks using this biothermochemistry method. The formation of these crosslinking structures is mainly due to the hydrogen bonding between a large number of carboxyl and hydroxyl functional groups on the surface of four crosslinking agents and hydroxyl and other functional groups on the surface of $Ti_3C_2T_x$ [45–47]. However, different

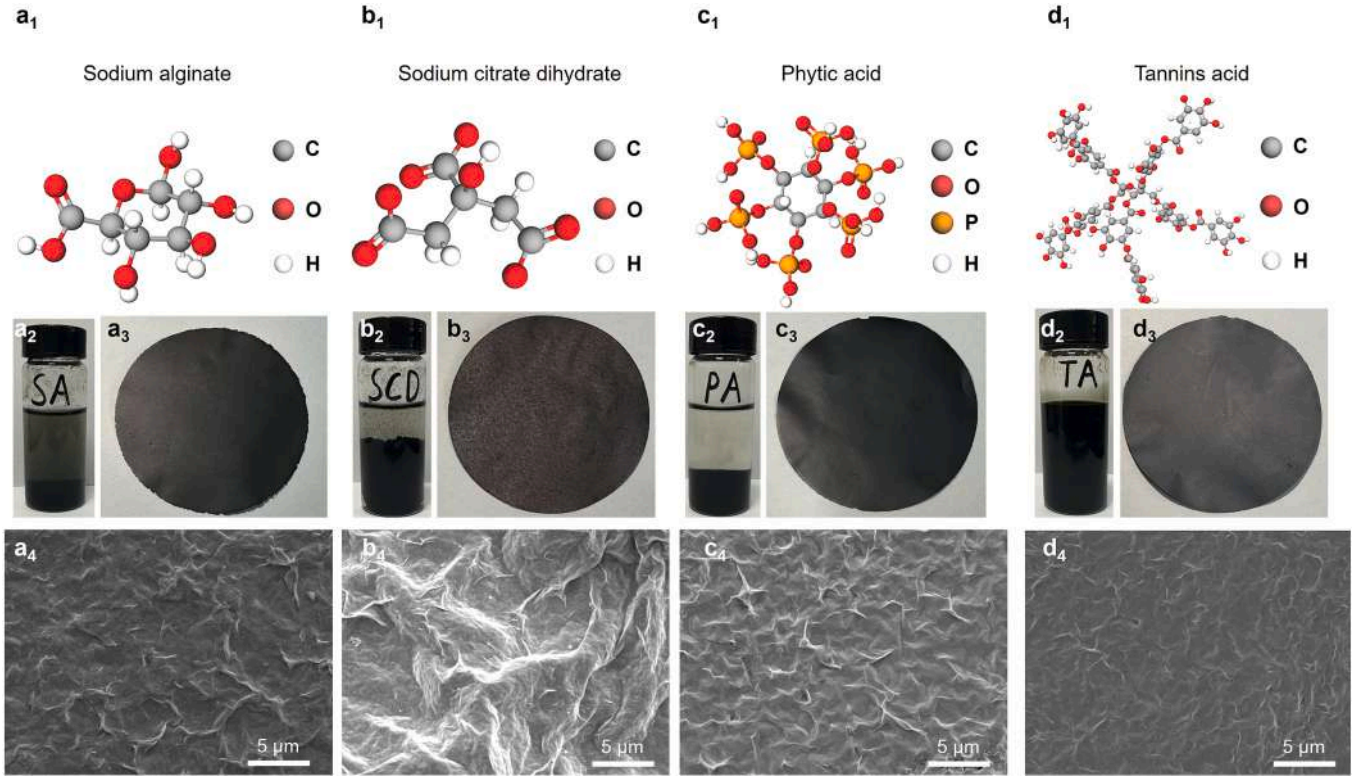

Fig. 3. 3D-MX constructed with another four crosslinking reagents. (a_1-a_4) 3D-MX-SA. (b_1-b_4) 3D-MX-SCD. (c_1-c_4) 3D-MX-PA. (d_1-d_4) 3D-MX-TA.

amounts of oxidized particles and cracks were observed on the surface of these $Ti_3C_2T_x$ (Figure S7), corresponding to structural damage. In comparison, the interlayer spacing of 3D-MX-G was larger and the nanosheets were smoother, so we conducted further research on it.

SEM and TEM images of t-MX and 3D-MX-G were displayed in Fig. 4 and Figure S8. Fig. 4a shows the structural diagram of P-MX and 3D-MX-G after long-term storage. The P-MX structure without glutathione protection was destroyed, producing TiO_2 and amorphous carbon while the formation of the 3D crosslinked structure and the reduction in the number of exposed Ti atoms made $Ti_3C_2T_x$ resist the attack of water and oxygen (Fig. 4b). Oxidized particles (white dotted lines) had appeared on the surface of t-MX after only one day of storage (Fig. 4c). And the degree of damage to the nanosheet increased after 21 days with the formation of a large amount of amorphous carbon (Fig. 4d). The colloidal solution of t-MX turned white only after 30 days, indicating complete structural destruction (Figure S8a-c). In contrast, glutathione provided excellent protection and greatly slowed $Ti_3C_2T_x$ oxidation with a storage time of over 550 days in water, showing strong oxidation protection effect (Figure S8d-f). Fig. 4e shows the crosslinked smooth surface of 3D-MX-G without the presence of TiO_2 particles. The surface of the nanosheets remained relatively intact and clean after 21 days (Fig. 4f). Then, we tested the XRD of t-MX and 3D-MX-G after being stored in an aqueous solution environment for several days, and the results directly showed that 3D-MX-G maintained strong antioxidant capacity within 15 days, while t-MX without crosslinked produced more TiO_2, indicating structural damage (Figure S9). Furthermore, Fig. 4g shows the contact angle of films of P-MX, t-MX and 3D-MX-G stored in an air environment for different times. The contact angle of P-MX was approximately 68.2°. The contact angle of t-MX decreased to 35.4° after biothermal treatment. However, the contact angle of t-MX increased to 48.1° and 59.6°, respectively after 7 days and 14 days, indicating the declined hydrophilicity of $Ti_3C_2T_x$. In contrast, the contact angle change of 3D-MX-G film was not obvious within 14 days, proving its strong stability. The reason why 3D-MX-G has such strong antioxidant ability is that after forming stable Ti-N bonds, removing some unstable surface functional groups, and forming a wide range of crosslinked structures, it can significantly resist water molecules and oxygen attacks, maintain long-term stability of the surface structure, and thus have excellent antioxidant ability.

Interestingly, compared to P-MX, the time for 3D-MX-G solution to be filtered into films were reduced from 5 h to 3 min (Video S1 and S2), mainly due to the larger interlayer spacing of 3D-MX-G. Similar to 2D materials such as graphene, $Ti_3C_2T_x$ is prone to self-stacking, resulting in a slow speed of vacuum filtration membrane formation, which greatly affects the efficiency of further expanding production in the future. Therefore, the ultra-fast vacuum filtration and film formation speed of 3D-MX-G exhibits great application potential.

Besides, the formation of 3D crosslinked structure also changed the electrical properties of $Ti_3C_2T_x$. The conductivity test results showed that the conductivity of P-MX film was 1229.5 S cm^{-1}, which decreased to 241.3 S cm^{-1} after being heated and placed for one day and continued to decline to a minimum of 137.7 S cm^{-1} in the next two weeks (Figure S10a). The continuous decrease in conductivity indicated the continuous progress of structural damage of $Ti_3C_2T_x$. Compared to P-MX, the conductivity of 3D-MX-G also decreased about 254.7 S cm^{-1} but remained stable over the next two weeks. The decrease in conductivity was due to the reduction of functional groups on the surface of $Ti_3C_2T_x$ after heating treatment, as well as structural damage, resulting in a decrease in hydrogen bonds. The reduction of the "bridge" structure reduced the speed of electron transfer. The formation of the 3D was beneficial for electron transfer to some extent. The conductivity of 3D-MX-G remained almost unchanged indicating excellent stability of the structure. We also studied the effect of film thickness on conductivity. Figure S10b shows the conductivity of P-MX and 3D-MX-G films with different thicknesses. The conductivity of P-MX increased from 90 S cm^{-1} to 640 S cm^{-1} and then decreases to 286 S cm^{-1} as the film thickness increased. The occurrence of this phenomenon was attributed to initially, an increase in the number of nanosheets to good electrical contact and therefore to the increased conductivity, while the stacked phenomenon in thickened $Ti_3C_2T_x$ films leads to the declined conductivity. For 3D-MX-G, its conductivity increased with the increase in film thickness because more crosslinked networks promoted electron transfer to some extent.

Based on the excellent hydrophilicity and conductivity, the supercapacitive properties of t-MX and 3D-MX-G were further studied using a three-electrode system in 1 M H_2SO_4 electrolyte. We first explored the optimal reaction parameters for 3D-MX-G: the addition concentration was 0.05 M, the reaction temperature was 75 ℃ and the reaction time was 12 h (Fig. 5a-c). Excessive glutathione content might lead to close interlayer proximity and then reduced capacitance. The crosslinking effect between $Ti_3C_2T_x$ and glutathione at low temperatures was unsatisfied due to the lack of enough reaction dynamics. The variation tendency in electrochemical capacitance of 3D-MX-G at higher temperatures was not apparent (Fig. 5b). Fig. 5d shows the CV curves of t-

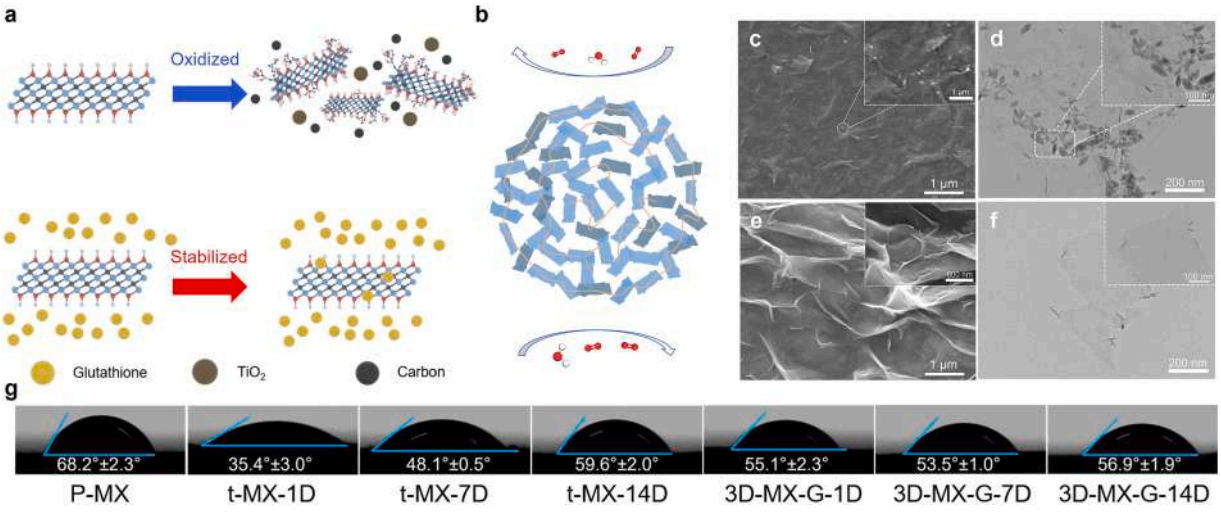

Fig. 4. On-shelf stability and structural stability. (a) Schematic diagram of structural changes of P-MX and 3D-MX-G after a period of time. (b) The formation of the 3D crosslinked structure blocked the attack of water and oxygen. (c) SEM image of P-MX stored in water for 1 day. (d) TEM image of P-MX stored in water for 21 days. (e) SEM image of 3D-MX-G stored in water for 1 day. (f) TEM image of P-MX stored in water for 21 days. (g) Contact angle changes of P-MX and 3D-MX-G stored in air for a period of time.

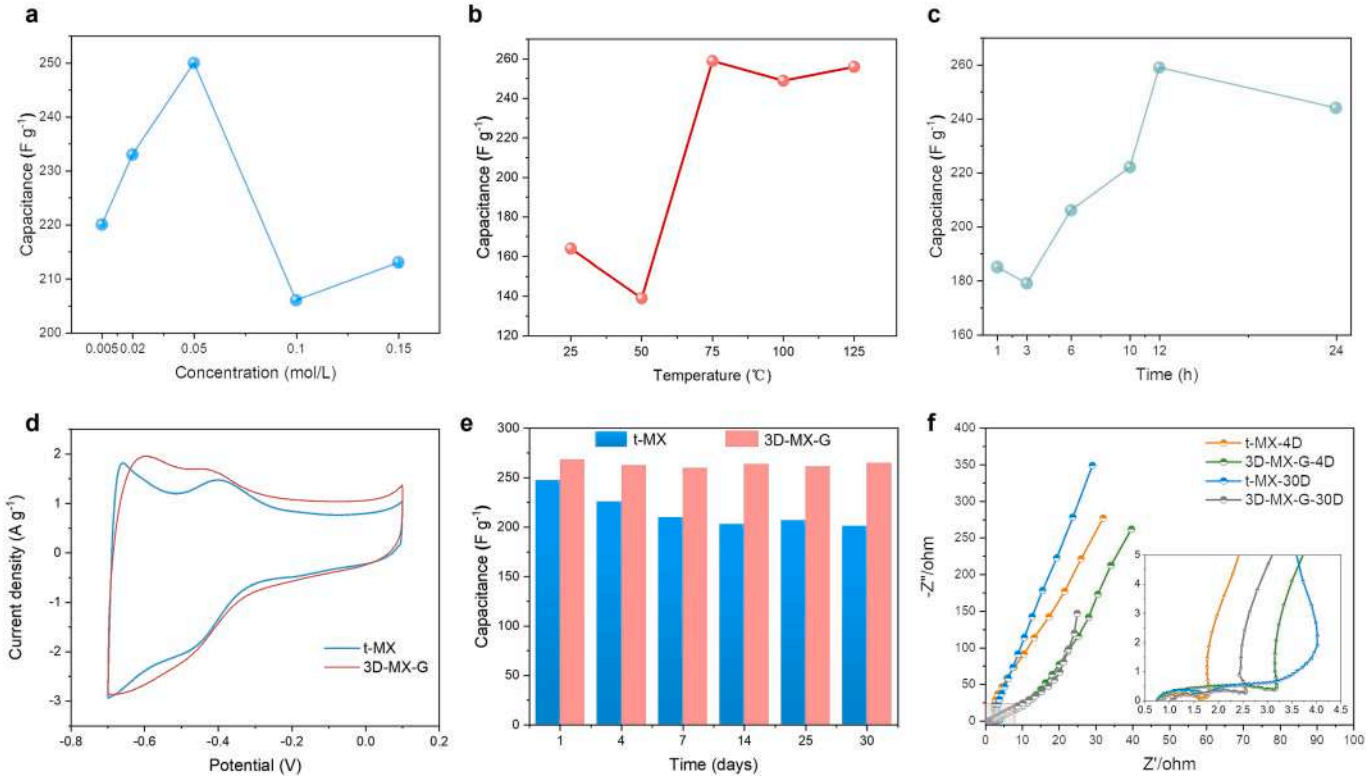

Fig. 5. Electrochemical performance of t-MX and 3D-MX-G films in a three-electrode system. (a-c) Mass capacitance of 3D-MX-G treated at different temperatures, times, and concentrations of glutathione. (d) CV curves of t-MX and 3D-MX-G at 5 mV s^{-1} after 4 days in air. (e) Gravimetric capacitance of t-MX and 3D-MX-G after storage in air for a period of time. (f) EIS plots of t-MX and 3D-MX-G after storage in air for a period of time.

MX and 3D-MX-G at a scan rate of 5 mV s^{-1}. 3D-MX-G displayed two couples of redox peaks and a larger integral area, consistent with a larger specific capacitance (268.5 F g^{-1} vs 247.5 F g^{-1} at 1 A g^{-1}). Compared to t-MX, the CV curve of 3D-MX-G was closer to rectangles with increasing scanning rate, indicating its better reversibility (Figure S11a and S11b). And the approximate triangular shape of the GCD curve of 3D-MX-G shows no significant voltage drop, indicating low internal resistance (Figure S11c).

Fig. 5e shows the electrochemical stability test results of t-MX and 3D-MX-G. The specific capacitance of 3D-MX-G had hardly decreased after 30 days of storage in air, maintaining at about 265 F g^{-1} at 1 A g^{-1}, showing excellent long-term stability. In contrast, the specific capacitance of t-MX gradually decreased from 247.5 F g^{-1} to about 201 F g^{-1} at 1 A g^{-1}, and the decrease became insignificant after about 14 days. This was because the unprotected $Ti_3C_2T_x$ was attacked by oxidation factors, resulting in massive structural damage and a gradual decrease in capacity. A large amount of TiO_2 and amorphous carbon accumulating on the surface of $Ti_3C_2T_x$ after 14 days reduced the oxidation degradation rate. Fig. 5f shows that the Nyquist diagram of 3D-MX-G exhibits excellent electrical conductivity at high frequencies and excellent charge transfer characteristics [48–50]. As a result, this 3D crosslinked structure formed by biothermochemistry method simultaneously solves the problems of self-stacking and oxidative degradation of $Ti_3C_2T_x$, while greatly improving the efficiency of film preparation, and therefore shows broad application prospects.

4. Conclusion

In conclusion, a variety of $Ti_3C_2T_x$ with 3D crosslinking structure are constructed by a novel biothermochemistry method, in which bioagents are combined with $Ti_3C_2T_x$ through electrostatic and/or the formation of Ti-N and S-S chemical bonds. On the one hand, 3D crosslinking effect expands the interlayer spacing and reduces self-stacking issue; On the other hand, bioagents reduce the number of exposed Ti atoms and effectively prevent the oxidation of $Ti_3C_2T_x$ MXene. Impressively, 3D-MX exhibits extraordinary antioxidant capacity as revealed by extremely-long on-shelf stability up to 550 days. In practical, as used as an electrode material for supercapacitors, 3D-MX-G exhibits high specific capacitance and excellent stability. This work solves the problems of self-stacking and oxidative degradation of $Ti_3C_2T_x$ and provides an excellent solution for exploring the further application and long-term preservation of $Ti_3C_2T_x$.

Declaration of Competing Interest

The authors declare that they have no known competing financial interests or personal relationships that could have appeared to influence the work reported in this paper.

Data availability

Data will be made available on request.

Acknowledgements

This work was supported by the National Natural Science Foundation of China (Nos. 51977185) and the Sichuan Science and Technology Program (No. 2023NSFSC0441). We are thankful to the Analytical and Testing Center of Southwest Jiaotong University for providing the SEM and XRD measurements.

Appendix A. Supplementary data

Supplementary data to this article can be found online at https://doi.org/10.1016/j.apsusc.2023.158183.

References

[1] M. Inagaki, F. Kang, Graphene derivatives: Graphane, fluorographene, graphene oxide, graphyne and graphdiyne, J. Mater. Chem. A 2 (2014) 13193–13206, https://doi.org/10.1039/C4TA01183J.

[2] Yecun Wu, Jingyang Wang, Yanbin Li, Jiawei Zhou, Bai Yang Wang, Ankun Yang, Lin-Wang Wang, Harold Y. Hwang, and Yi Cui, Observation of an intermediate state during lithium intercalation of twisted bilayer MoS_2. Nat. Commun. 13 (2022) 3008, doi: https://doi.org/10.1038/s41467-022-30516-z.

[3] M.B. Erande, M.S. Pawar, D.J. Late, Humidity sensing and photodetection behavior of electrochemically exfoliated atomically thin-layered black phosphorus nanosheets, ACS Appl. Mater. Interfaces 8 (2016) 11548–11556, https://doi.org/10.1021/acsami.5b10247.

[4] P.u. Shi, Z. Wang, Y. Xie, J. Fan, X.u. Zhong, Y. Wang, H. He, X. Zhang, W. Yang, H. Zhang, Origin and regulation of self-discharge in MXene supercapacitors, Adv. Funct. Mater. 33 (2023) 2208715, https://doi.org/10.1002/adfm.202208715.

[5] Y. Wang, F.u. Jimin, X.u. Jiangang, H.u. Haibo, D. Ho, Atomic plasma grafting: Precise control of functional groups on $Ti_3C_2T_x$ MXene for room temperature gas sensors, ACS Appl. Mater. Interfaces 15 (2023) 12232–12239, https://doi.org/10.1021/acsami.2c22609.

[6] K.e. Li, J. Zhao, A. Zhussupbekova, C.E. Shuck, L. Hughes, Y. Dong, S. Barwich, S. Vaesen, I.V. Shvets, M. Möbius, W. Schmitt, Y. Gogotsi, V. Nicolosi, 4D printing of MXene hydrogels for high-efficiency pseudocapacitive energy storage, Nat. Commun. 13 (2022) 6884, https://doi.org/10.1038/s41467-022-34583-0.

[7] M. Naguib, O. Mashtalir, J. Carle, V. Presser, L.u. Jun, L. Hultman, Y. Gogotsi, M. W. Barsoum, Two-dimensional transition metal carbides, ACS Nano 6 (2012) 1322–1331, https://doi.org/10.1021/nn204153h.

[8] Q. Wang, Y. Zhou, X. Zhao, K. Chen, G.u. Bingni, T. Yang, H. Zhang, W. Yang, J. Chen, Tailoring carbon nanomaterials via a molecular scissor, Nano Today 36 (2021) 101033, https://doi.org/10.1016/j.nantod.2020.101033.

[9] M. Ma, W. Tao, X. Liao, S.i. Chen, Y. Shi, H. He, X.u. Wang, Cellulose nanofiber/MXene/FeCo composites with gradient structure for highly absorbed electromagnetic interference shielding, Chem. Eng. J. 452 (2023) 139471, https://doi.org/10.1016/j.cej.2022.139471.

[10] M.-J. Tao, S.-Q. Cheng, X.-L. Han, F. Yi, Y.u. Run-Hao Li, Y.S. Rong, Y.i. Liu, Alignment of MXene based membranes to enhance water purification, J. Membrane Sci. 662 (2022) 120965, https://doi.org/10.1016/j.memsci.2022.120965.

[11] Viet Phuong Nguyen, Mikyung Lim, Kyung-Shik Kim, Jae-Hyun Kim, Ji Su Park, Jong Min Yuk, and Seung-Mo Lee, Drastically increased electrical and thermal conductivities of Pt-infiltrated MXenes. J. Mater. Chem. A. 9 (2021) 10739–10746, https://doi.org/10.1039/D1TA00331C.

[12] Z. Fan, Y. Wang, Z. Xie, X.u. Xueqing, Y. Yuan, Z. Cheng, Y. Liu, A nanoporous MXene film enables flexible supercapacitors with high energy storage, Nanoscale 10 (2018) 9642–9652, https://doi.org/10.1039/C8NR01550C.

[13] J. Zhang, N.K.D. Hegh, A.S. Ken, G.G. Usman, S.i. Qin, I. Jurewicz, W. Yang, J. M. Razal, Freezing titanium carbide aqueous dispersions for ultra-long-term, ACS Appl. Mater. Interfaces 12 (2020) 34032–34040, https://doi.org/10.1021/acsami.0c06728.

[14] Fanjie Xia, Junchao Lao, Ruohan Yu, Xiahan Sang, Jiayan Luo, Yu Li, and Jinsong Wu, Ambient oxidation of Ti_3C_2 MXene initialized by atomic defects. Nanoscale 11 (2019) 23330–23337, https://doi.org/10.1039/C9NR07236E.

[15] Yoonjeong Chae, Seon Joon Kim, Soo-Yeon Cho, Junghoon Choi, Kathleen Maleski, Byeong-Joo Lee, Hee-Tae Jung, Yury Gogotsi, Yonghee Lee, and Chi Won Ahn, An investigation into the factors governing the oxidation of two-dimensional Ti_3C_2 MXene. Nanoscale 11 (2019) 8387–8393, https://doi.org/10.1039/C9NR00084D.

[16] H. Ghassemi, W. Harlow, O. Mashtalir, M. Beidaghi, M.R. Lukatskaya, Y. Gogotsi, M.L. Taheri, In situ environmental transmission electron microscopy study of oxidation of two-dimensional Ti_3C_2 and formation of carbon-supported TiO_2, J. Mater. Chem. A 2 (2014) 14339–14343, https://doi.org/10.1039/C4TA02583K.

[17] C.J. Zhang, S. Pinilla, N. McEvoy, C.P. Cullen, B. Anasori, E. Long, S.-H. Park, A. Seral-Ascaso, A. Shmeliov, D. Krishnan, C. Morant, X. Liu, G.S. Duesberg, Y. Gogotsi, V. Nicolosi, Oxidation stability of colloidal two-dimensional titanium carbides (MXenes), Chem. Mater. 29 (2017) 4848–4856, https://doi.org/10.1021/acs.chemmater.7b00745.

[18] Sehyun Doo, Ari Chae, Daesin Kim, Taegon Oh, Tae Yun Ko, Seon Joon Kim, Dong-Yeun Koh, and Chong Min Koo, Mechanism and kinetics of oxidation reaction of aqueous $Ti_3C_2T_x$ suspensions at different pHs and temperatures. ACS Appl. Mater. Interfaces 13 (2021) 22855−22865, https://doi.org/10.1021/acsami.1c04663.

[19] K. Maleski, V.N. Mochalin, Y. Gogotsi, Dispersions of two-dimensional titanium carbide MXene in organic solvents, Chem. Mater. 29 (2017) 1632–1640, https://doi.org/10.1021/acs.chemmater.6b04830.

[20] W.u. Xianhong, Z. Wang, Y.u. Mengzhou, L. Xiu, J. Qiu, Stabilizing the MXenes by carbon nanoplating for developing hierarchical nanohybrids with efficient lithium storage and hydrogen evolution capability, Adv. Mater. 29 (2017) 1607017, https://doi.org/10.1002/adma.201607017.

[21] M. Shang, X.i. Chen, B. Li, J. Niu, A fast charge/discharge and wide-temperature battery with a germanium oxide layer on a Ti_3C_2 MXene matrix as anode, ACS Nano 14 (2020) 3678–3686, https://doi.org/10.1021/acsnano.0c00556.

[22] T.S. Mathis, K. Maleski, A. Goad, A. Sarycheva, M. Anayee, A.C. Foucher, K. Hantanasirisakul, C.E. Shuck, E.A. Stach, Y. Gogotsi, Modified MAX phase synthesis for environmentally stable and highly conductive Ti_3C_2 MXene, ACS Nano 15 (2021) 6420–6429, https://doi.org/10.1021/acsnano.0c08357.

[23] Y. Lee, S.J. Kim, Y. Kim, Y. Lim, Y. Chae, B. Lee, Y. Kim, H. Han, Y. Gogotsi, C. W. Ahn, Oxidation-resistant titanium carbide MXene films, J. Mater. Chem. A 8 (2020) 573–581, https://doi.org/10.1039/C9TA07036B.

[24] G.S. Lee, T. Yun, H. Kim, I.H. Kim, J. Choi, S.H. Lee, H.J. Lee, H.S. Hwang, J. G. Kim, D. Kim, H.M. Lee, C.M. Koo, S.O. Kim, Mussel inspired highly aligned $Ti_3C_2T_x$ MXene film with synergistic enhancement of mechanical strength and ambient stability, ACS Nano 14 (2020) 11722–11732, https://doi.org/10.1021/acsnano.0c04411.

[25] F. Yang, D. Hegh, D. Song, J. Zhang, A.S. Ken, Z.W. Usman, P. Zhang, W. Ma, W. Yang, S.i. Qin, J.M. Razal, A nitrogenous pre-intercalation strategy for the synthesis of nitrogen-doped $Ti_3C_2T_x$ MXene with enhanced electrochemical capacitance, J. Mater. Chem. A 9 (2021) 6393–6401, https://doi.org/10.1039/D0TA11907E.

[26] X. Zhao, A. Vashisth, E. Prehn, W. Sun, S.A. Shah, T. Habib, Y. Chen, Z. Tan, J. L. Lutkenhaus, M. Radovic, M.J. Green, Antioxidants unlock shelf-stable $Ti_3C_2T_x$ (MXene) nanosheet dispersions, Matter 1 (2019) 513–526, https://doi.org/10.1016/j.matt.2019.05.020.

[27] C. Wu, B. Unnikrishnan, I. P. Chen, S.G. Harroun, H. Chang, C. Huang, Excellent oxidation resistive MXene aqueous ink for micro-supercapacitor application, Energy Storage Mater. 25 (2020) 563–571, https://doi.org/10.1016/j.ensm.2019.09.026.

[28] V. Natu, J.L. Hart, M. Sokol, H. Chiang, M.L. Taheri, M.W. Barsoum, Edge capping of 2D-MXene sheets with polyanionic salts to mitigate oxidation in aqueous colloidal suspensions, Angew. Chem. Int. Ed. 58 (2019) 12655–12660, https://doi.org/10.1002/anie.201906138.

[29] C. Zhang, J. Xiao, X. Zhang, X.u. Dexin, H. Gao, 3D crumpled $Ti_3C_2T_x$-xerogel architectures for optimized lithium storage, Electrochim. Acta 427 (2022) 140857, https://doi.org/10.1016/j.electacta.2022.140857.

[30] M. Peng, L.i. Wang, L. Li, X. Tang, B. Huang, H.u. Ting, K. Yuan, Y. Chen, Manipulating the interlayer spacing of 3D MXenes with improved stability and zinc-ion storage capability, Adv. Funct. Mater. 32 (2022) 2109524, https://doi.org/10.1002/adfm.202109524.

[31] K. Yang, M. Luo, D. Zhang, C. Liu, Z. Li, L. Wang, W. Chen, X. Zhou, $Ti_3C_2T_x$/carbon nanotube/porous carbon film for flexible supercapacitor, Chem. Eng. J. 427 (2022) 132002, https://doi.org/10.1016/j.cej.2021.132002.

[32] X. Wang, Y. Wang, D. Liu, X. Li, Y.u. Huanhao Xiao, M.X. Ma, G. Yuan, G. Chen, Opening MXene ion transport channels by intercalating PANI nanoparticles from the self-assembly approach for high volumetric and areal energy density supercapacitors, ACS Appl. Mater. Interfaces 13 (2021) 30633–30642, https://doi.org/10.1021/acsami.1c06934.

[33] Z. Wang, X.u. Zhong, H. Huang, X. Chu, Y. Xie, D.a. Xiong, C. Yan, H. Zhao, H. Zhang, W. Yang, Unraveling and regulating self-discharge behavior of $Ti_3C_2T_x$ MXene-based supercapacitors, ACS Nano 14 (2020) 4916–4924, https://doi.org/10.1021/acsnano.0c01056.

[34] Z.-W. Gao, W. Zheng, L.Y.S. Lee, Highly enhanced pseudocapacitive performance of vanadium-doped MXenes in neutral electrolytes, Small 15 (2019) 1902649, https://doi.org/10.1002/smll.201902649.

[35] A. Lipatov, M. Alhabeb, M.R. Lukatskaya, A. Boson, Y. Gogotsi, A. Sinitskii, Effect of synthesis on quality, electronic properties and environmental stability of individual monolayer Ti_3C_2 MXene Flakes, Adv. Electron. Mater. 2 (2016) 1600255, https://doi.org/10.1002/aelm.201600255.

[36] J. Halim, K.M. Cook, M. Naguib, P. Eklund, Y. Gogotsi, J. Rosen, M.W. Barsoum, X-ray photoelectron spectroscopy of select multi-layered transition metal carbides (MXenes), Appl. Surf. Sci. 362 (2016) 406–417, https://doi.org/10.1016/j.apsusc.2015.11.089.

[37] T. Yun, H. Kim, A. Iqbal, Y.S. Cho, G.S. Lee, M. Kim, S.J. Kim, D. Kim, Y. Gogotsi, S. O. Kim, C.M. Koo, Electromagnetic shielding of monolayer MXene assemblies, Adv. Mater. 32 (2020) 1906769, https://doi.org/10.1002/adma.201906769.

[38] L.i. Zhu, J. Lv, Y.u. Xianfeng, H. Zhao, C. Sun, Z. Zhou, Y. Ying, L. Tan, Further construction of MnO_2 composite through in-situ growth on MXene surface modified by carbon coating with outstanding catalytic properties on thermal decomposition of ammonium perchlorate, Appl. Surf. Sci. 502 (2020) 144171, https://doi.org/10.1016/j.apsusc.2019.144171.

[39] M. Han, J. Yang, J. Jiang, R. Jing, S. Ren, C. Yan, Efficient tuning the electronic structure of N-doped Ti-based MXene to enhance hydrogen evolution reaction, J. Colloid Interf. Sci. 582 (2021) 1099–1106, https://doi.org/10.1016/j.jcis.2020.09.001.

[40] P.u. Liuyue, J. Zhang, N.K.L. Jiresse, Y. Gao, H. Zhou, N. Naik, P. Gao, Z. Guo, N–doped MXene derived from chitosan for the highly effective electrochemical properties as supercapacitor, Adv. Compos. Hybrid MA. 5 (2022) 356–369, https://doi.org/10.1007/s42114-021-00371-5.

[41] J. Wang, Z. Zhang, X. Yan, S. Zhang, W.u. Zihao, Z. Zhuang, W.-Q. Han, Rational design of porous N-Ti_3C_2 MXene@CNT microspheres for high cycling stability in Li–S battery, Nano-Micro Lett. 12 (2020) 4, https://doi.org/10.1007/s40820-019-0341-6.

[42] Q. Li, T. Song, Z. Wang, X. Wang, X. Zhou, Q.i. Wang, Y. Yang, A general strategy toward metal sulfide nanoparticles confined in a sulfur-doped $Ti_3C_2T_x$ MXene 3D porous aerogel for efficient ambient N_2 electroreduction, Small 17 (2021) 2103305, https://doi.org/10.1002/smll.202103305.

[43] G. Li, S. Lian, F. Song, S. Chen, W.u. Zhenjun, X. Xie, N. Zhang, Surface chemistry and mesopore dual regulation by sulfur-promised high volumetric capacity of $Ti_3C_2T_x$ films for sodium-ion storage, Small 17 (2021) 2103626, https://doi.org/10.1002/smll.202103626.

[44] R.B. Rakhi, M.N. Bilal Ahmed, D.H. Hedhili, Anjum, H.N. Alshareef, Effect of postetch annealing gas composition on the structural and electrochemical properties of Ti_2CT_x MXene electrodes for supercapacitor applications, Chem. Mater. 27 (2015) 5314–5323, https://doi.org/10.1021/acs.chemmater.5b01623.

[45] H. Liu, Y. Liu, X.u. Dan, L. Chen, W. Guo, G.u. Tiantian, Y.u. Feng, G. Wang, 3D cross-linked $Ti_3C_2T_x$-Ca-SA films with expanded $Ti_3C_2T_x$ interlayer spacing as

freestanding electrode for all-solid-state flexible pseudocapacitor, J. Colloid Interf. Sci. 610 (2022) 295–303, https://doi.org/10.1016/j.jcis.2021.10.127.
[46] N. Gupta, R.K. Sahu, T. Mishra, P. Bhattacharya, Microwave-assisted rapid synthesis of titanium phosphate free phosphorus doped Ti_3C_2 MXene with boosted pseudocapacitance, J. Mater. Chem. A 10 (2022) 15794–15810, https://doi.org/10.1039/D2TA04061A.
[47] Z. Hao, S. Zhang, S. Yang, X. Li, Y. Gao, J. Peng, L. Li, L. Bao, X. Li, Bridged $Ti_3C_2T_X$ MXene film with superior oxidation resistance and structural stability for high-performance flexible supercapacitors, ACS Appl. Energy Mater. 5 (2022) 2898–2908, https://doi.org/10.1021/acsaem.1c03575.
[48] Y. Xie, H. Zhang, H. Huang, Z. Wang, X.u. Zhong, H. Zhao, Y. Wang, N. Chen, W. Yang, High-voltage asymmetric MXene-based on-chip micro-supercapacitors, Nano Energy 74 (2020) 104928, https://doi.org/10.1016/j.nanoen.2020.104928.
[49] Y. Wang, X. Chu, H. Zhang, C. Yan, G. Tian, W. Yang, X. Chen, H. Zhang, Hyper-conjugated polyaniline delivering extraordinary electrical and electrochemical properties in supercapacitors, Appl. Surf. Sci. 628 (2023) 157350, https://doi.org/10.1016/j.apsusc.2023.157350.
[50] X. Jiang, W.u. Xinzheng, Y. Xie, Z. Wang, J. Huang, Q.u. Yuanxiao, M.u. Dali, X. Zhang, W. Yang, H. Zhang, Additive engineering enables ionic-liquid electrolyte-based supercapacitors to deliver simultaneously high energy and power density, ACS Sustain. Chem. Eng. 11 (2023) 5685–5695, https://doi.org/10.1021/acssuschemeng.3c00213.